PAPER Nr.: 26

PRELIMINARY THREE-DIMENSIONAL CFD MODEL OF A HELICOPTER FUSELAGE

BY

T J KIRSTEN

AEROTEK, CSIR
PRETORIA, SOUTH AFRICA

TWENTIETH EUROPEAN ROTORCRAFT FORUM
OCTOBER 4 - 7, 1994 AMSTERDAM

Printed by the Technical Highschool Haarlem

PRELIMINARY THREE-DIMENSIONAL CFD MODEL OF A HELICOPTER FUSELAGE

T J Kirsten

CSIR, Aerotek, P.O.Box 395 Pretoria 0001, South Africa.

ABSTRACT

The design or modification of a helicopter must include the aerodynamic performance of the fuselage to ensure that the helicopter system performance is met or exceeded. Both experimental and numerical methods can be used to investigate this aerodynamic behaviour. As computational power increases, the use of more complex analysis tools becomes feasible. A CFD approach that can best address this type of problem is a three-dimensional Navier-Stokes formulation. The objective of this investigation was to develop three-dimensional CFD models to predict the aerodynamic performance of the Alouette III fuselage, the fuselage with the engine and the fuselage with an infra-red suppression cowl. An isolated fuselage was modelled which implies that a multitude of interaction effects were neglected. To demonstrate that this model can capture the dominant physical features of the flow, results on and around the fuselage are presented. The next goal was to validate the CFD prediction against experimental data. The validation was performed using one-fifth and full-scale aerodynamic coefficients of the Alouette III at various combinations of angle of attack and yaw. The lift and drag coefficients were compared to experimental data and this process demonstrated the accuracy with which these preliminary CFD models can predict the performance changes due to the modification of the fuselage. The accuracy can be improved through model upgrade, finer grid resolution and additional detailed validation.

NOMENCLATURE

Abbreviations

CFD	Computational Fluid Dynamics.
CAD	Computer Aided Design.
LSWT	Low Speed Wind Tunnel.
7mWT	7m Wind Tunnel.
TLNS	Thin Layer Navier-Stokes.
BO	Fuselage body only.
BE	Fuselage body and engine.
BC	Fuselage body and cowl.

Variables

α	Angle of attack relative to the datum line of the model (degrees).
β	Angle of yaw relative to the vertical symmetry plane of the model (degrees).
ρ	density.
u	x component of the velocity.
v	y component of the velocity.
(x,y)	Cartesian co-ordinates in the physical domain.
e	total energy.
γ	ratio of specific heats.
Re	Reynolds number.
Pr	Prandtl number.
μ	dynamic viscosity (a constant plus the turbulent eddy viscosity).
l	reference length.
t	time.
τ	time in generalised curvilinear co-ordinates.

τ	*viscous stress terms.*
$\xi = \xi(x, y, t)$	one of the co-ordinates in the generalised curvilinear co-ordinates.
$\eta = \eta(x, y, t)$	one of the co-ordinates in the generalised curvilinear co-ordinates.

Subscripts and superscripts

∞	free stream quantities.
t	partial derivative with respect to time = ∂_t.
x	partial derivative with respect to $x = \partial_x$.
y	partial derivative with respect to $y = \partial_y$.
xx	second partial derivative with respect to $x \wedge x = \partial_{xx}$.
xy	second partial derivative with respect to $x \wedge y = \partial_{xy}$.
yy	second partial derivative with respect to $y \wedge y = \partial_{yy}$.
$(\hat{})$	in the generalised curvilinear co-ordinate system.
$(\sim)$	non-dimensional variable.

1 INTRODUCTION

The design or modification of a helicopter must include the aerodynamic performance of the fuselage to ensure that the helicopter system performance is met or exceeded. Fuselage drag is usually a substantial component of the total helicopter drag and the fuselage also plays a large role in helicopter stability. Both experimental and numerical methods can be used to investigate the aerodynamic behaviour of a helicopter fuselage. Experimental investigations can include wind tunnel tests and full-scale tests. Wind tunnel tests allow for controlled investigations, but are unable to model some of the important phenomena which can only be obtained from flight tests. Aerodynamic effects can also be modelled using a suitable three-dimensional numerical program.

As computational power increases, the use of more complex analysis tools becomes feasible. The techniques employed to analyse helicopter fuselages in forward flight have progressed from classical aerodynamics, eg [1], to panel methods, eg [3] to [6], to the most recent Navier-Stokes methods. A number of investigations have also studied the interaction process between the various helicopter components, schematically depicted in figure 1, eg [7] to [9]. The inviscid models are usually based on panel methods for the fuselage displacement and a vortex distribution for the wake. It would be more useful if the method employed could capture the wake effects automatically, ie performing a viscous analysis. A CFD method that can address this sort of problem is a three-dimensional Navier-Stokes formulation. This approach is capable of predicting the viscous flow that is present on the fuselage, including separation. The separated region can be a dominant factor in the determination of the aerodynamic coefficients of the fuselage.

To enable this investigation to commence the fuselage was assumed to be isolated. This implies that the multitude of effects [7] due to the main rotor, tail rotor, engine, landing gear and all other external objects were neglected. The complete fuselage was modelled in order to simulate the effects of yaw and angle of attack simultaneously. If only angle of attack is required a half-model can be used but this will limit any further development, as most of the interaction effects on the fuselage are asymmetric. When the engine and cowl components are combined with the fuselage, regions are created which would necessitate highly distorted grids. To overcome this problem, either an unstructured grid or a multi-blocking CFD approach can be used. Aerotek is in the process of developing the latter option, but this development was not complete when the current investigation was carried out. A structured single block approach was used and the necessary approximations were made.

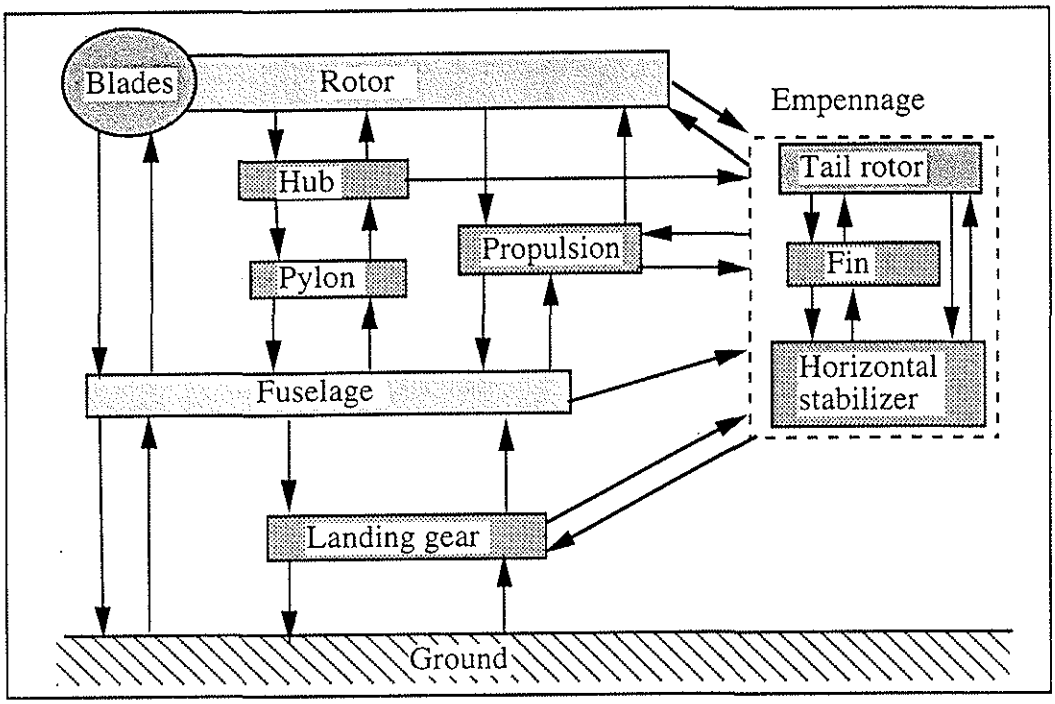

Figure 1: Schematic of the helicopter aerodynamic interactions.

The objective of this investigation was to develop three-dimensional CFD models to predict the aerodynamic performance of the Alouette III fuselage, the fuselage with the engine and the fuselage with an infra-red suppression cowl. These numerical predictions were compared with experimental measurements. The Alouette III was used as a vehicle to develop the technology because a number of fuselage modifications had been made to the Alouette III and these had been experimentally evaluated. The fuselage geometry was obtained from a CAD model and the operating conditions were calculated from the wind tunnel test conditions. The CFD solver and models that were employed will be described in Section 2. The grid generation and geometric approximations are described in Section 3.

To demonstrate that this model can capture the dominant physical features of the flow, results will be presented for the flow field on and around the fuselage. The main objective of this preliminary model development is to validate the CFD prediction against experimental data. The major portion of the comparison will be made with one-fifth scaled aerodynamic coefficients of the Alouette III. Full-scale data will also be used for comparative purposes, but the amount of this data available is small. CFD validation will be performed at various combinations of angle of attack and yaw. The lift and drag coefficients will be compared to the experimental data and this process will demonstrate the accuracy with which the CFD model can predict the performance changes due to the modification of the fuselage, see Section 4.

2 CFD MODEL

A TLNS code was used to simulate the three different Alouette III fuselage geometric arrangements. The implicit approximate factorization CFD code used in this investigation is based on the algorithm described in the publications of Beam and Warming [10] and Pulliam [11]. Implicit schemes have become popular because of their unconditional linear stability. In practice, for nonlinear systems the stability bounds encountered for implicit schemes are much less stringent than for explicit schemes. These schemes produce large linear systems of algebraic equations which are computationally expensive to solve. Making use of an implicit time

difference and a second order spatial difference to the two-dimensional Euler equations produces a large coupled block system of equations which even for a moderately sized mesh is too costly to solve, hence the development of the approximate factorization scheme by Beam and Warming [10].

The derivation shown below starts with the strongly conservative formulation of the two-dimensional Navier-Stokes equations in Cartesian co-ordinates. The extension to three-dimensions is simple from this two-dimensional description. The equations in non-dimensional form are:

$$\partial_t Q + \partial_x E + \partial_y F = Re^{-1}(\partial_x E_v + \partial_y F_v) \tag{1}$$

where:

$$Q = \begin{bmatrix} \rho \\ \rho u \\ \rho v \\ e \end{bmatrix}, \quad E = \begin{bmatrix} \rho u \\ \rho u^2 + p \\ \rho uv \\ u(e+p) \end{bmatrix}, \quad F = \begin{bmatrix} \rho v \\ \rho uv \\ \rho v^2 + p \\ v(e+p) \end{bmatrix}$$

and

$$E_v = \begin{bmatrix} 0 \\ \tau_{xx} \\ \tau_{xy} \\ f_4 \end{bmatrix}, \quad F_v = \begin{bmatrix} 0 \\ \tau_{xy} \\ \tau_{yy} \\ g_4 \end{bmatrix}$$

with:

$$\tau_{xx} = \mu(4u_x - 2v_y)/3$$

$$\tau_{xy} = \mu(u_y + v_x)$$

$$\tau_{yy} = \mu(-2u_x + 4v_y)/3$$

$$f_4 = u\tau_{xx} + v\tau_{xy} + \mu Pr^{-1}(\gamma - 1)^{-1}\partial_x a^2$$

$$g_4 = u\tau_{xy} + v\tau_{yy} + \mu Pr^{-1}(\gamma - 1)^{-1}\partial_y a^2$$

Pressure is related to the conservative flow variable, Q, by the equation of state

$$p = (\gamma - 1)\left(e - \frac{1}{2}\rho(u^2 + v^2)\right) \tag{2}$$

The choice of non-dimensional parameters is based on those selected by Pulliam [11].

$$\tilde{\rho} = \frac{\rho}{\rho_\infty}, \quad \tilde{u} = \frac{u}{a_\infty}, \quad \tilde{v} = \frac{v}{a_\infty}, \quad \tilde{e} = \frac{e}{\rho_\infty a_\infty^2} \tag{3}$$

The speed of sound for an ideal fluid is,

$$a^2 = \gamma p/\rho. \tag{4}$$

Assuming a reference length, l, usually taken as some characteristic physical length (ie the fuselage length), time t scales as $\bar{t} = ta/l$.

The Euler equations can be transformed from Cartesian co-ordinates to general curvilinear co-ordinates where:

$$\begin{aligned} \tau &= t \\ \xi &= \xi(x, y, t) \\ \eta &= \eta(x, y, t). \end{aligned} \tag{5}$$

The transformations are chosen so that the grid spacing in the curvilinear space is uniform and of unit length. This produces a computational space ξ and η which is a rectangular domain and which has a regular uniform mesh so that standard unweighted differencing schemes can be used in the numerical formulation. The original Cartesian space will be referred to as the physical domain. With this construction a single computational code can be produced for a wide variety of physical geometries and grid systems. Chain rule expansions are used to represent the Cartesian derivatives ∂_x and ∂_y of equation (1) in terms of the curvilinear derivatives where in matrix form

$$\begin{bmatrix} \partial_t \\ \partial_x \\ \partial_y \end{bmatrix} = \begin{bmatrix} 1 & \xi_t & \eta_t \\ 0 & \xi_x & \eta_x \\ 0 & \xi_y & \eta_y \end{bmatrix} \begin{bmatrix} \partial_\tau \\ \partial_\xi \\ \partial_\eta \end{bmatrix} \tag{6}$$

Applying equation (6) to the Euler equations, equation (1), we have

$$\begin{aligned} &\partial_\tau Q + \xi_t \partial_\xi Q + \eta_t \partial_\eta Q \\ &+\xi_x \partial_\xi E + \eta_x \partial_\eta E + \xi_y \partial_\xi F + \eta_y \partial_\eta F \\ &= Re^{-1}(\eta_x \partial_\xi E_v + \eta_x \partial_\eta E_v + \xi_y \partial_\xi F_v + \eta_y \partial_\eta F_v) \end{aligned} \tag{7}$$

The rest of the CFD model details have been excluded for the sake of brevity. The capability to extend the fuselage-only model to include other components of the helicopter is demonstrated by the addition of the engine and the engine cowl to the fuselage, see figures 2 and 3 respectively. The approximate regions can be seen where the fuselage surface is blended into the engine and cowl surfaces respectively. In later developments these fuselage models can be extended to include the other areas of interaction, as depicted in figure 1. Each configuration advance requires a different level of development, either simple boundary condition modification and new grid generation or re-writing the solver. The ultimate goal would be to have a model which simulates all the helicopter sub-systems effects.

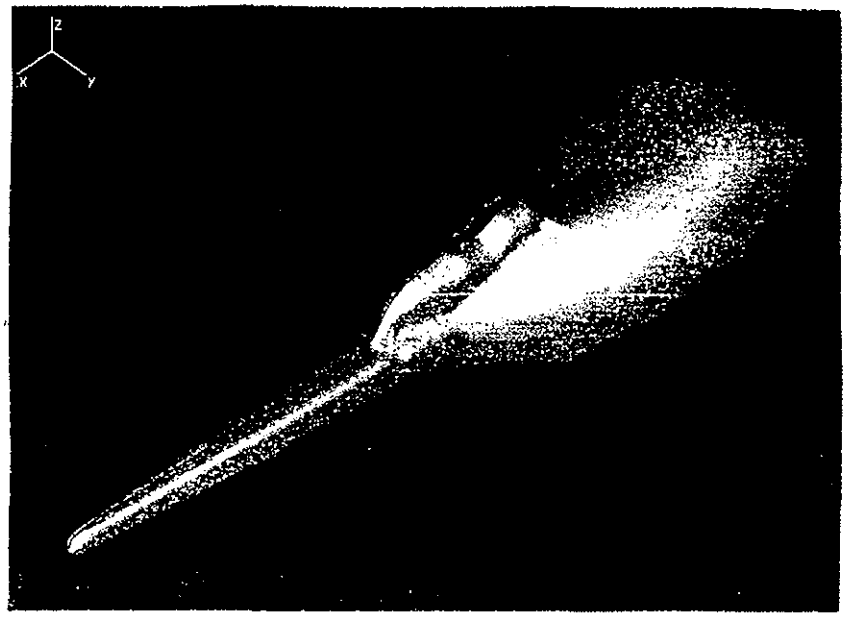

Figure 2: Alouette III fuselage and engine surface as obtained from CAD.

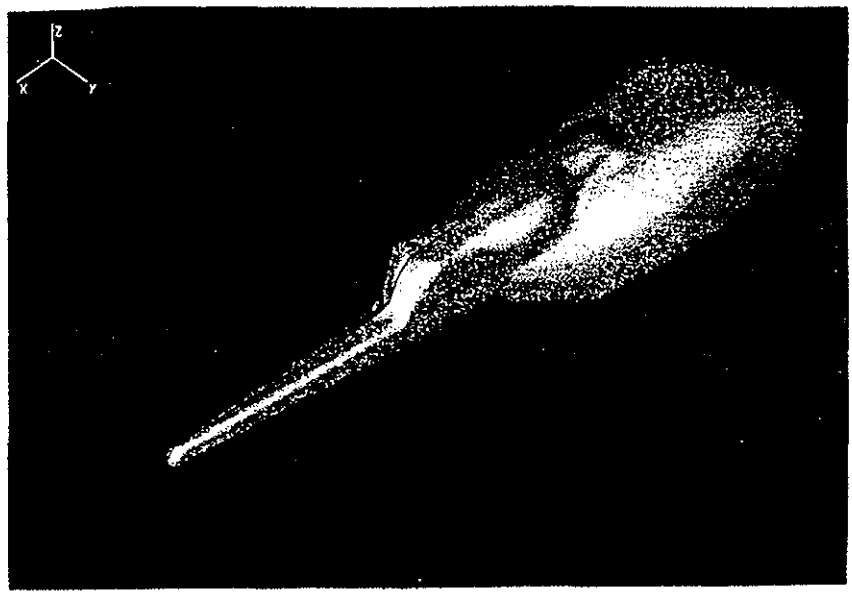

Figure 3: Alouette III fuselage and cowl surface as obtained from CAD.

3 GRID GENERATION

The geometric definition of the Alouette III fuselage was extracted in parallel streamwise slices through the geometric CAD definition. Aerotek's three-dimensional elliptic surface and field grid generation code, based on Thompson [12], was used to generate an O-O grid. Three different grids were generated to simulate the three cases considered:

1. Alouette III fuselage only.
2. Alouette III fuselage with the engine.
3. Alouette III fuselage with a cowl designed for infra-red suppression.

When the components are combined with the fuselage, regions are created which would necessitate highly distorted grids, and to overcome this problem, either an unstructured grid or a multi-blocking CFD approach could be used. Aerotek is in the process of developing the latter option, but this development was not complete when the current investigation was carried out. To avoid grid distortion without having an advanced CFD approach available, approximations had to be made. These approximations involved removing enclosed regions between the fuselage and the engine, smoothing regions of large surface slope changes (eg 90° bends), and smoothing regions of highly complex detail (eg engine casing), see figures 2 and 3.

The number of grid nodes used in the three co-ordinate directions is 90x37x40 for the body only and 90x50x40 for the other two cases. 90 grid points were used from the nose to the tail of the fuselage. 37 grid points were used to define the surface around the fuselage, one cell being in the overlap region. The models with the modified fuselage shape require more grid points in order to capture the new definition adequately and therefore 50 were used instead of 37. 40 grid points were used from the fuselage surface to the far-field boundary. The fuselage-only grid therefore uses a total of 133200 grid points and extends just over 2 fuselage lengths into the free-stream. The perpendicular size of the first grid cell adjacent to the fuselage surface is 0.00084 fuselage lengths.

An oblique view of the three grids used for this investigation are given in Figures 4 to 6, side and top views are presented in figure 7. The body and engine grid, figure 5, shows the grid refinement that was necessary in the engine region. The approximations mentioned above are also clearly visible, the region between the engine and the fuselage is not modelled, the engine intake and exhaust has been faired-off similar to the method used for wind tunnel models and the engine casing shape has been smoothed. Effectively, a blanket has been thrown over the engine and allowed to drape down the sides of the body. These approximations were necessary and it is shown that the dominant effect of the engine was captured satisfactorily. All these modifications were performed using the CAD model to ensure surface smoothness and to have a CAD record of the modifications.

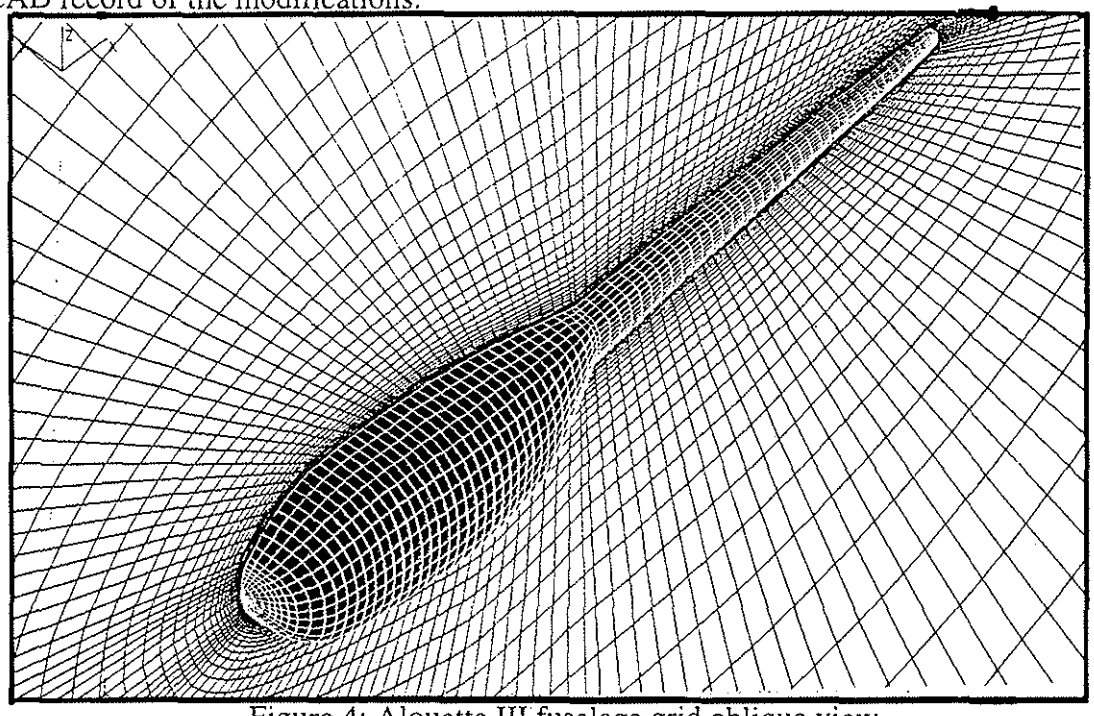

Figure 4: Alouette III fuselage grid oblique view.

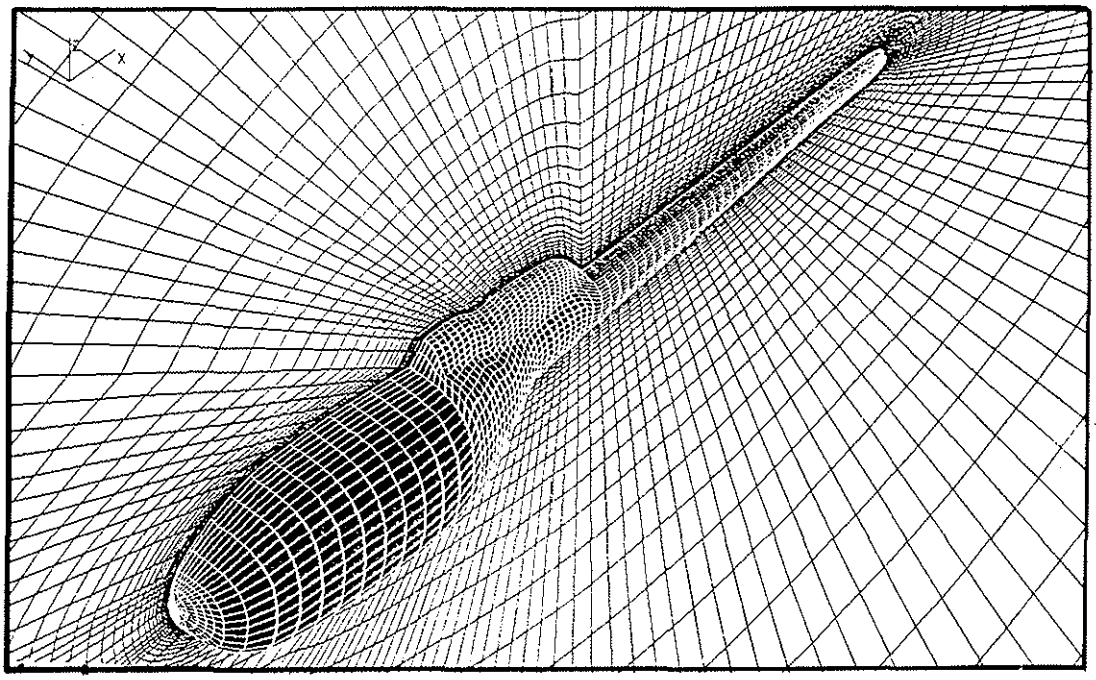

Figure 5: Alouette III fuselage and engine grid oblique view.

The most obvious feature of the fuselage and cowl model shown in figure 6 is the greater size of the cowl. The cowl was designed to enclose the main rotor drive shaft, engine and infra-red suppression system. This model required significantly less approximation due to it being an aerodynamic cowl fitting smoothly onto the fuselage and not an engine jutting out of the fuselage. The main approximation was made in the engine intake and exhaust regions, and the most significant grid shearing can be seen to be downstream of the exhaust. The final two grids consist of 180000 grid nodes, 35% more than the fuselage model in order to capture the increased geometric complexity.

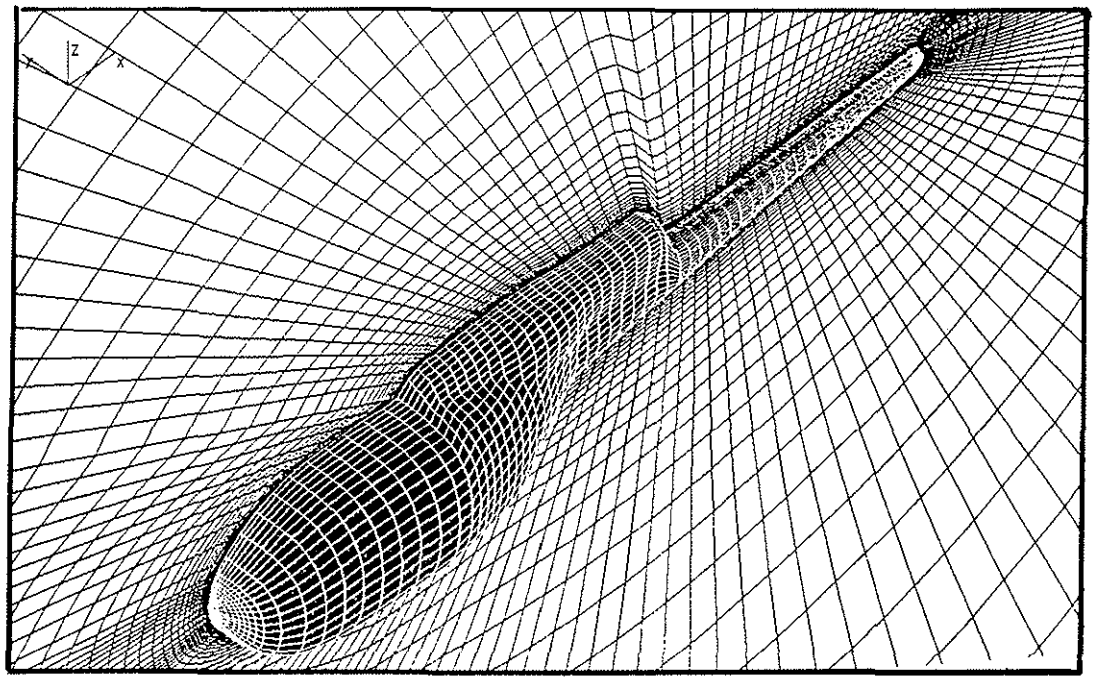

Figure 6: Alouette III fuselage and cowl grid oblique view.

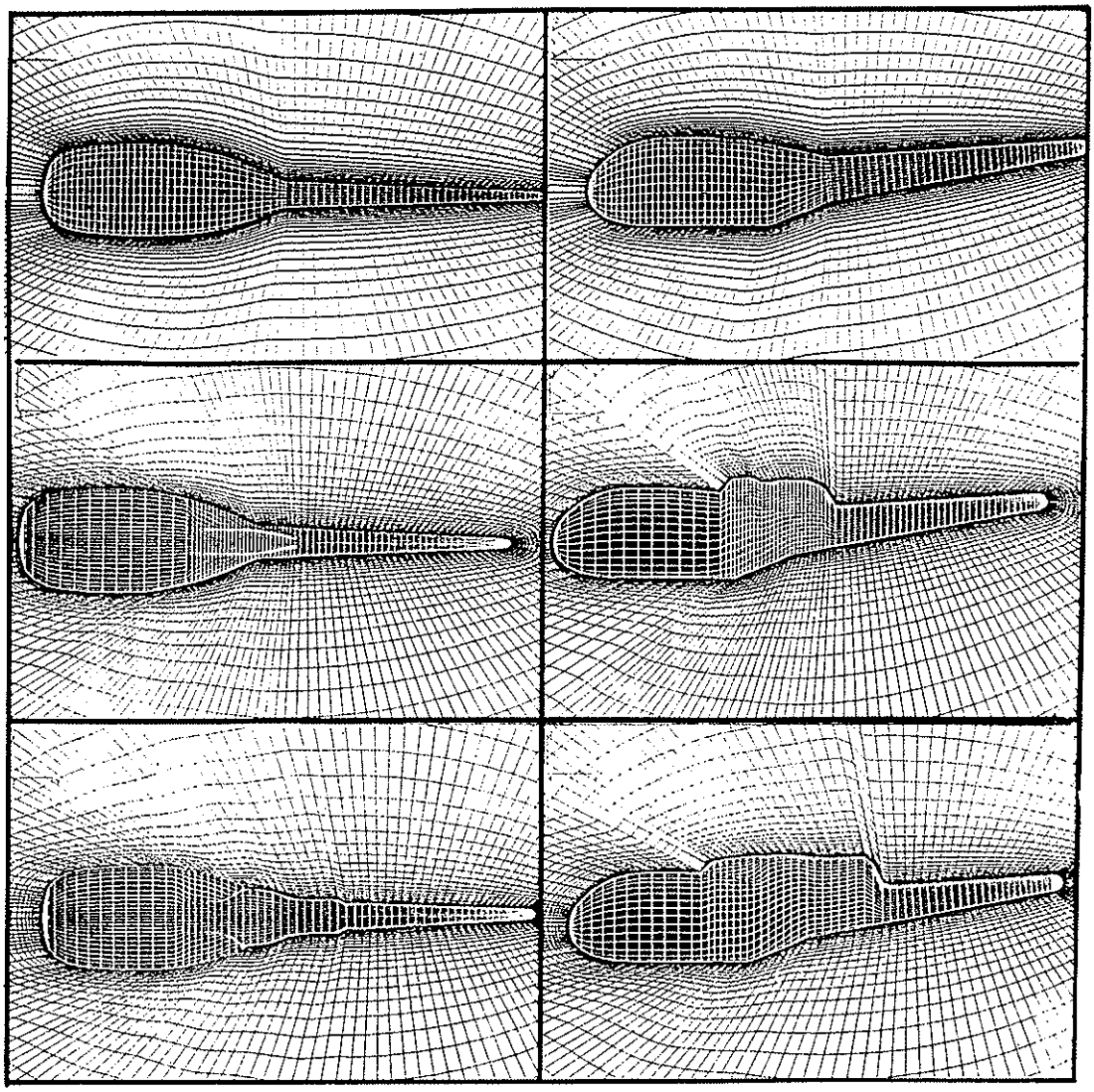

Figure 7: Side and top view: a) Alouette III fuselage, b) including engine and c) including cowl.

4 RESULTS

Some characteristic flow solutions will be presented first. These have been selected to highlight that the dominant physical features have been successfully captured within the accuracy of the grid resolution and CFD method. It is difficult to effectively display the results in black and white, as is the case here, but the comparative features between the results is still discernible. The results presented here correspond to the conditions of α=-6° and β=0°. Firstly, the pressure distribution on the side of the helicopter fuselage and vertical symmetry plane through the fuselage is presented in figure 8 for each of the three cases. The modification of the fuselage surface pressure distribution is marked in the vicinity of the engine and cowl, but this effect is relatively localised as is expected. This effect can also be seen in the pressure distribution on the fuselage itself and it is this localised modification of the flow field that causes the changes in the aerodynamic behaviour of the helicopter fuselage.

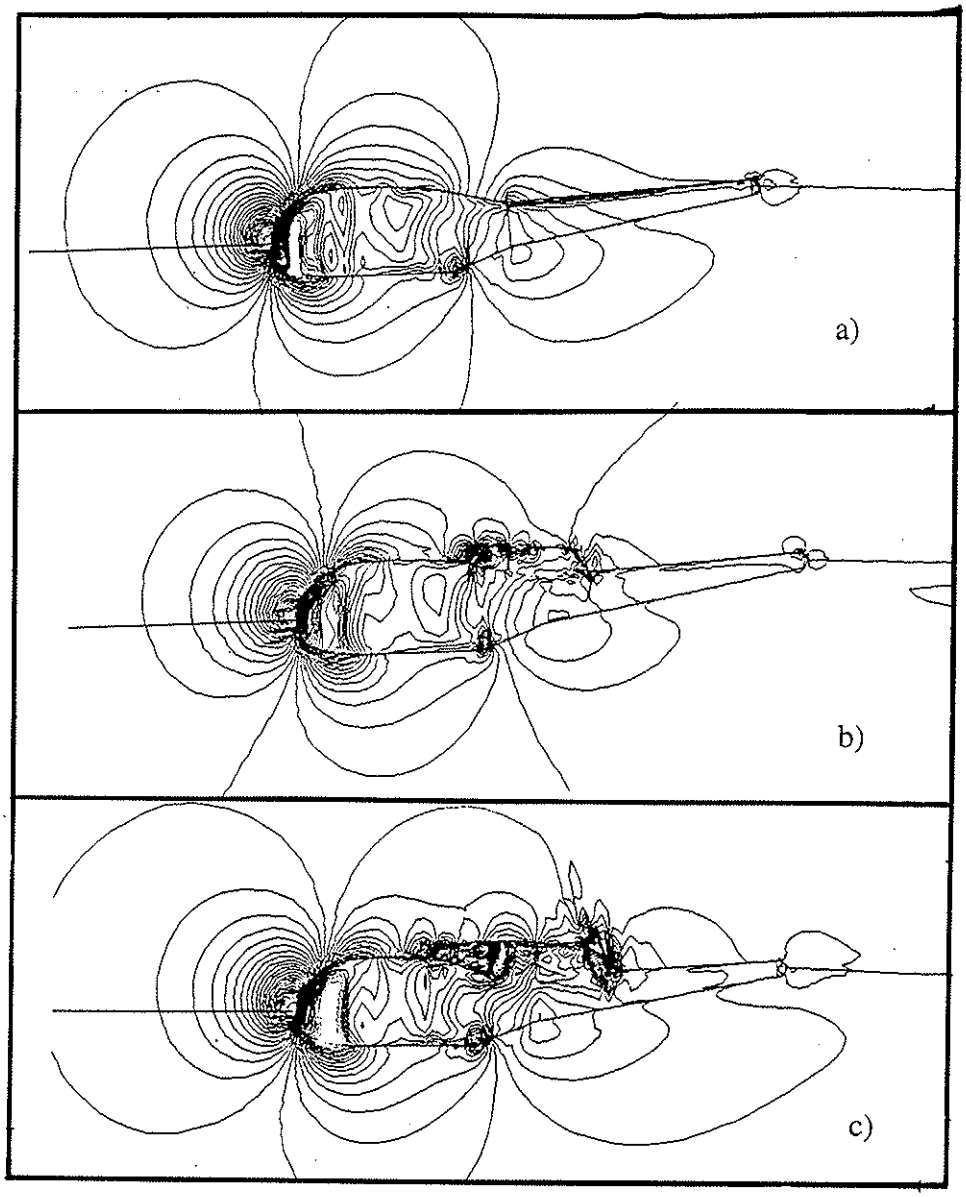

Figure 8: Pressure distribution on the side of the helicopter fuselage and vertical symmetry plane through the fuselage: a) BO, b) BE and c) BC.

Figure 9 depicts the velocity vector field on the vertical symmetry plane through the fuselage. Each result has a small zone of recirculating air on the lower surface of the fuselage upstream of the intersection of the fuselage and the tail boom. The separation is caused by the large adverse pressure gradient due to the rapidly reducing fuselage size. The flow re-attaches further downstream before the tail boom. The zone of recirculating air does not change markedly between the three cases, but the worst seems to be the fuselage alone, which is expected, as it has the largest fuselage size reduction. The surface above the fuselage for the three cases has very different flow patterns. The local acceleration around the engine and cowl obstruction is clearly visible, as well as the wake downstream of the obstruction.

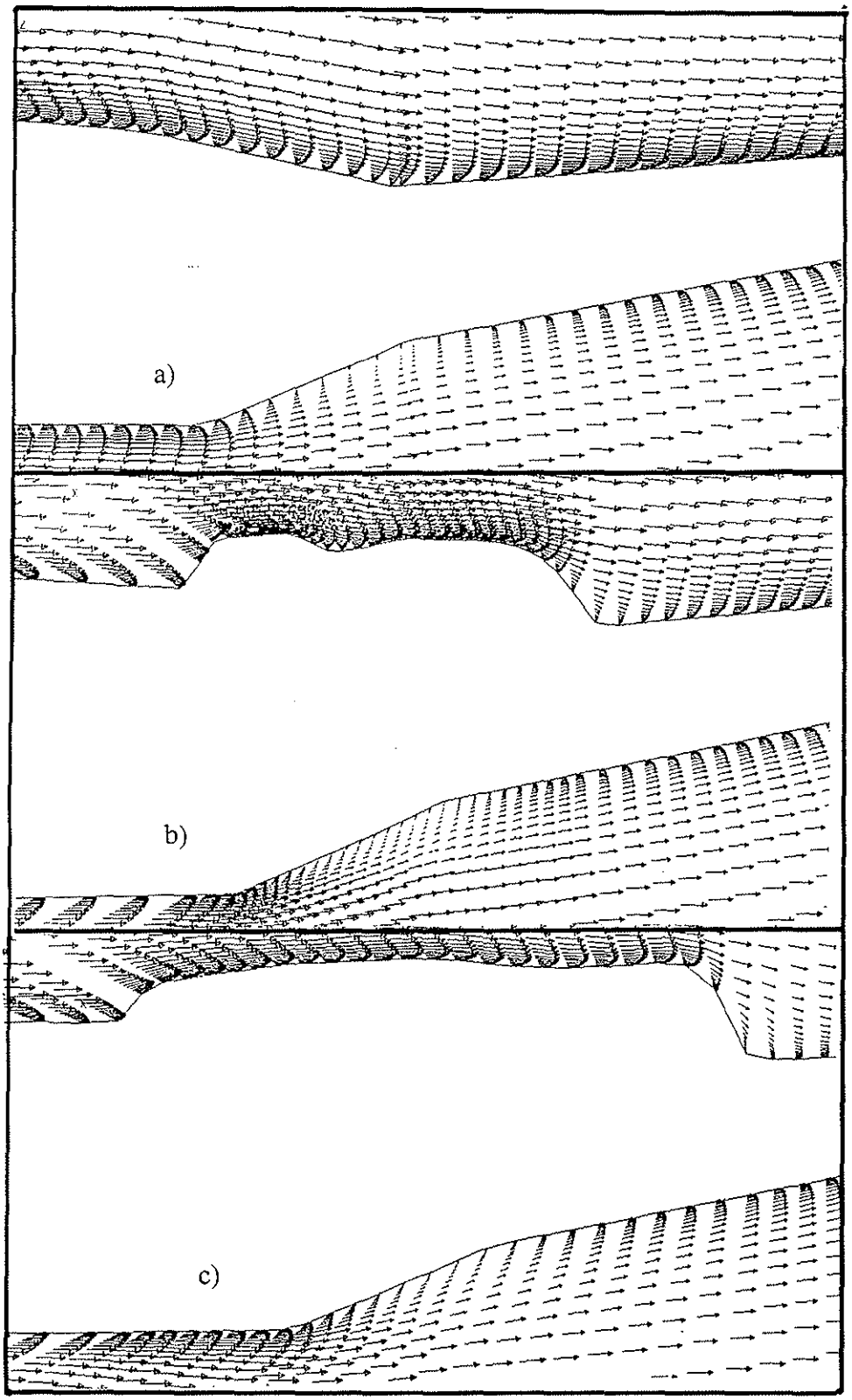

Figure 9: Velocity vector field on the vertical symmetry plane through the fuselage: a) BO, b) BE and c) BC.

Another view of the CFD data which helps to highlight the differences in the three flow fields is a plan view. The reason for this is that the engine and cowl are above the fuselage and therefore more differences will be present around these modifications. The pressure distribution on the upper surface of the helicopter fuselage and the horizontal plane through the maximum width of the fuselage for each of the three cases is shown in figure 10. The modification of the fuselage surface pressure distribution is marked in the vicinity of the engine and cowl. This effect is relatively localised. Forward of the mid-fuselage station the flow pattern seems to be unchanged, but from this station rearward each case has a different pressure distribution. The effect is greater downstream due to the blockage effect of the engine and cowl. The engine and cowl both cause areas of localised acceleration and deceleration as compared to the relatively unobstructed flow over the fuselage-alone case. It is this localised modification to the flow field that contributes to the changes in the aerodynamic behaviour of the helicopter fuselage.

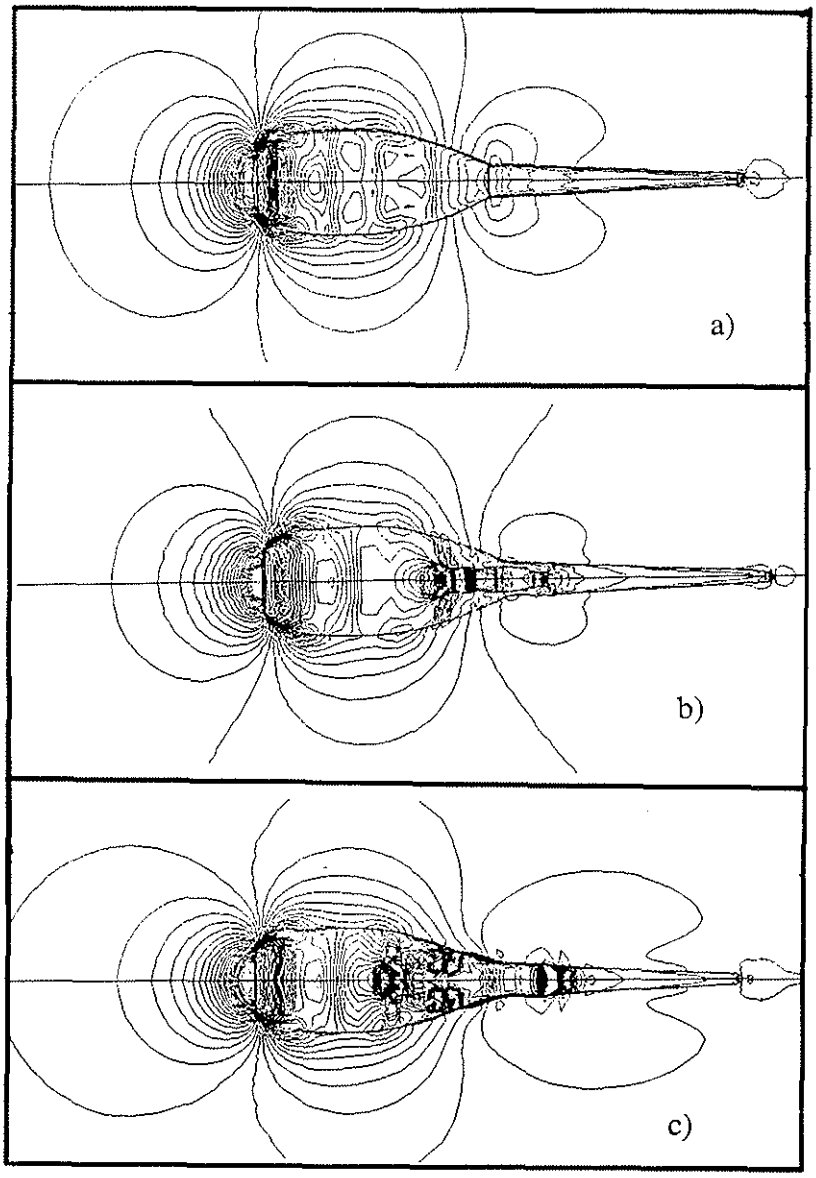

Figure 10: Pressure distribution on the upper surface of the helicopter fuselage and the horizontal plane through the maximum width of the fuselage: a) BO, b) BE and c) BC.

Figure 11 depicts the velocity vector field close to the upper surface of the helicopter fuselage and the horizontal plane through the maximum width of the fuselage for each of the three cases. The velocity vectors could not be shown on the fuselage surface as they are all zero, a viscous non-slip boundary condition. Thus, the vectors have been drawn one plane above the fuselage surface. This plane is still in the viscous boundary layer therefore the magnitude of the velocity vectors are of no significance, but they do indicate the direction of the flow close to the fuselage. This flow direction on the upper surface of the fuselage clearly indicates the effect of the engine and cowl. The fuselage alone, figure 11a, has flow moving straight down the fuselage up to the tail boom and then the flow moves outwards over the tail boom due to the flow having to move around the upward sloping tail boom. The flow field for the engine and cowl cases, figures 11b and 11c, also have the velocity vectors pointing down the fuselage, but the effect of the obstruction is felt upstream and the flow starts to flow outward and around the obstruction. The acceleration in small areas around the obstruction is also visible. The flow in the cowl case, figure 20c, can be seen to be forced sideways beyond the horizontal extent of the fuselage and the tail boom. The field velocities in each of the three cases are relatively similar and this highlights the limited nature of the influence of the engine and cowl.

A wide range of CFD results were obtained for different angles of attack and yaw. To demonstrate the CFD prediction capability, some selected results will be given with α=-12° and β=10°. The main difference between these results, figure 12, and the previous results, figures 8 to 11, is that they were obtained with a yaw angle of 10° and not symmetrical flight. The non-symmetrical pressure distribution around the fuselage alone model has been presented in figure 12a. It is the summation of this pressure distribution around the fuselage that gives rise to the side force. Figure 12b, presents a similar view to the previous figure, but shows the velocity field around the intersection of the fuselage and tail boom. The two sides of the fuselage have very different flow patterns, the windward side has a larger velocity level than the leeward side. The leeward side boundary layer also seems to be closer to separation. Away from the fuselage the flow angle of 10° can be seen.

The effect of yaw on the engine and cowl is also of interest and this effect is expected to be significant, because the largest dimension of the engine or the cowl are aligned with the flow direction. Figure 13 shows the velocity vectors around the engine and cowl with β=10°. The flow can be seen to be moving across the fuselage at an angle. This flow pattern will result in an increase in the side force with changing β as compared to the fuselage alone.

All of the results demonstrate the capability of the prediction method to calculate the expected effect of the engine and cowl on the fuselage. The next objective of this investigation was to validate these CFD models using experimental data. The main comparison was made with the one-fifth scaled aerodynamic coefficient data from the Aerotek LSWT. The model was built in such a manner that the following tests could be performed: body only, body & tail, body & tail & engine, body & tail & main undercarriage, body & tail & nose undercarriage, complete airframe less tail, and complete airframe. These tests were performed prior to this investigation and unfortunately no tests were performed for the body and engine, but by making an assumption that the components of the model have little influence on one another this result can be estimated from:

[body] + ([body & tail & engine] - [body & tail])

The experimental conditions were as follows:

Tunnel dynamic pressure (q)	1,033 q_t
Tunnel nominal dynamic pressure (q_t)	800 mm water
Equivalent air speed	115 m/s

Reynolds number based on model fuselage length	12,6 million
Reference area, full scale rotor disc	95,0 m^2
Reference dimension, full scale rotor radius	5,5 m

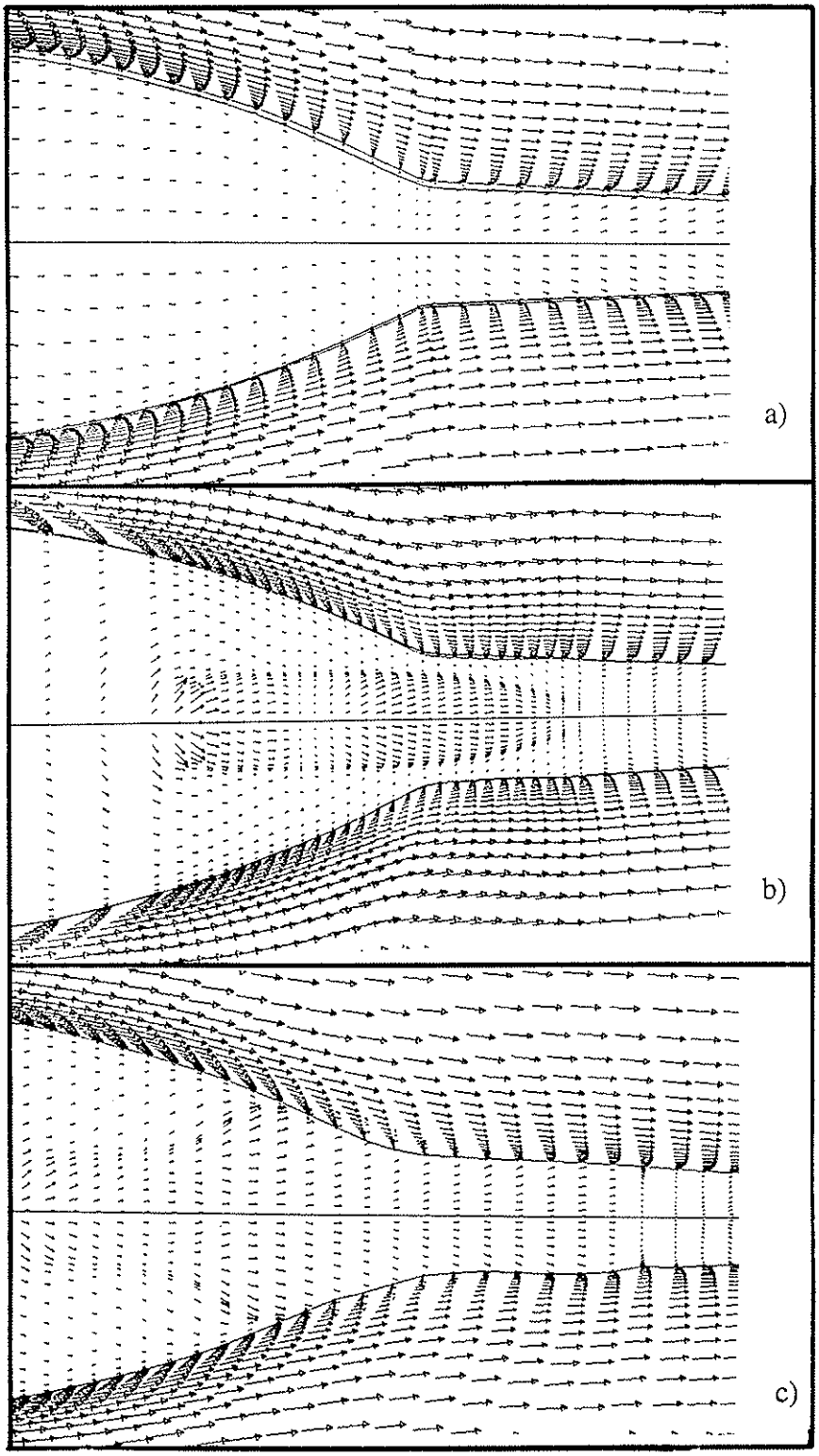

Figure 11: Velocity vector field close to the upper surface of the helicopter fuselage and on the horizontal plane through the maximum width of the fuselage: a) BO, b) BE and c) BC.

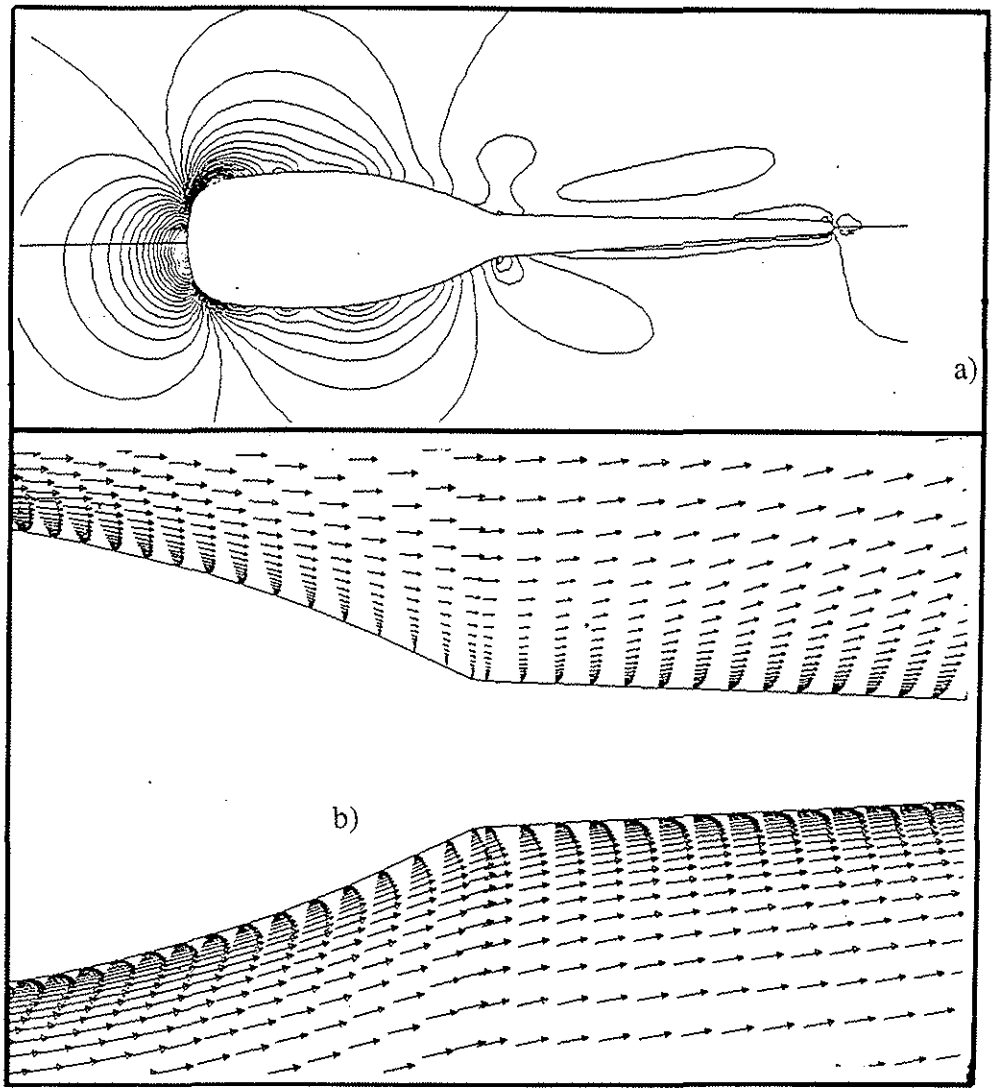

Figure 12: Pressure contour plot (a) and velocity vector plot (b) on the horizontal plane through the maximum width of the fuselage (BO).

These conditions translate to the following CFD input:

Ambient temperature	278.39 K
Speed of sound	344 m/s
Mach number	0,3443
Reynolds number based on CFD model fuselage length	63 million
Ratio of specific heats	1,4
Prandtl number	0.72

Only aerodynamic coefficients will be used for this validation exercise and in the future, data could also be extracted in particular areas of the model as demonstrated above. For example, if the designer requires the pressure or velocity field near the engine intake, it can be easily extracted. Selected CFD results will now be compared with the experimental data to demonstrate the accuracy of the CFD data.

The first validation result presented is the lift coefficient variation with angle of attack under zero yaw conditions, figure 14. All the results have similar trends and exhibit very small differences between the various configurations and methods. This is an expected result as this fuselage is not intended to be a lift generating body. The best accuracy was obtained for the body with the engine. The fuselage-only case is not predicted as accurately, but the experimental

model had a main rotor drive shaft to which the wind tunnel balance was mounted and the CFD model did not model this which is a possible cause for the discrepancy. The discrepancy is reduced when the engine is present, as the engine nullifies the effect of the main rotor drive shaft.

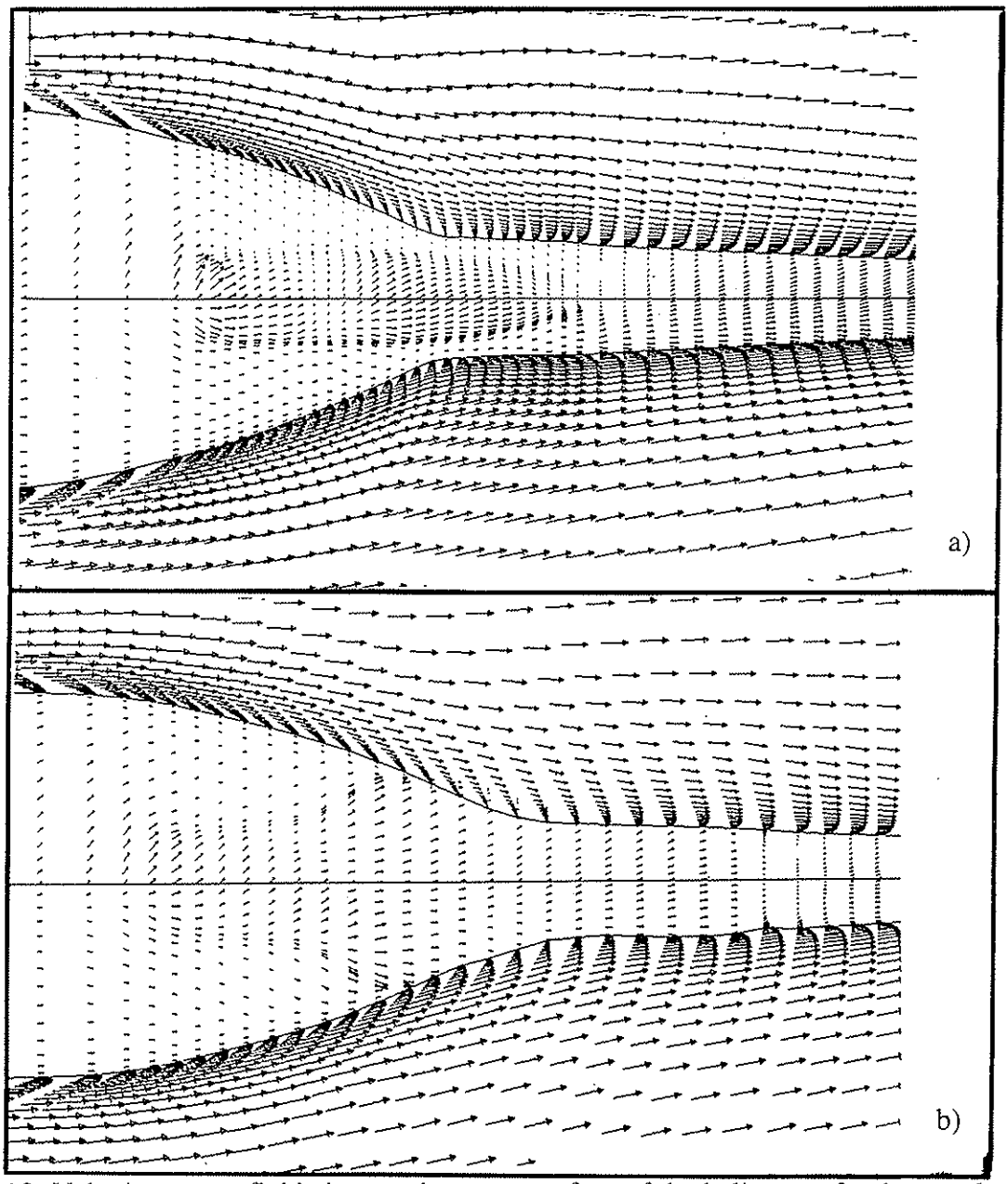

Figure 13: Velocity vector field close to the upper surface of the helicopter fuselage and on the horizontal plane through the maximum width of the fuselage: a) BE and b) BC.

The second validation result presented is the drag coefficient variation with angle of attack under zero yaw conditions, figure 15. Once again, all the results have similar trends, but relative magnitudes in each case is different. The CFD solution consistently under-predicts the coefficient of drag and the best accuracy was obtained for the body with the engine. The possible reason for this effect was explained above and the under-prediction of the drag was expected due to the relatively low grid density, idealised surface finish and inadequate turbulence modelling for separated regions (Baldwin-Lomax). The trends are surprisingly accurate and possibly the skin friction drag is also too low, which would cause each CFD drag curve to rise by an equivalent amount. The extraction of skin friction on a relatively coarse grid is known

to give rise to inaccuracies and possibly this value should be extracted by using a different velocity gradient technique. Various other coefficients can also be used for validation, ie side force and pitching moment, but due to a lack of space these have not been included here.

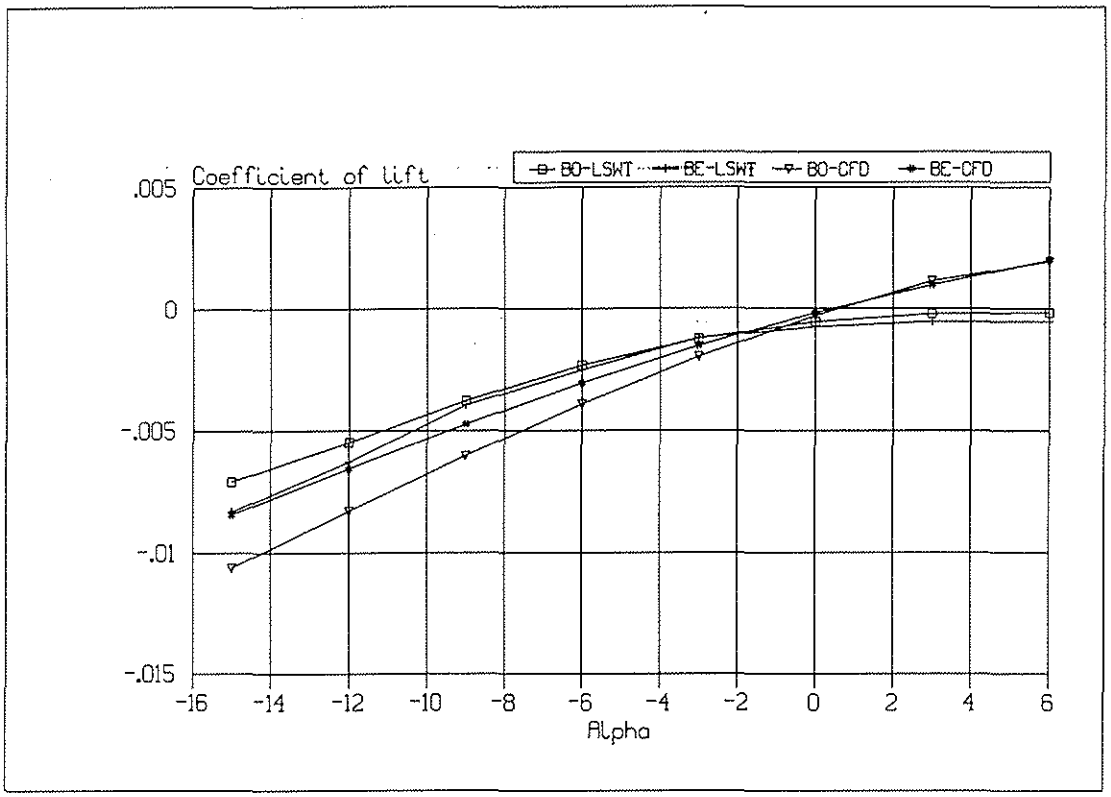

Figure 14: Coefficient of lift variation with angle of attack for the zero yaw conditions.

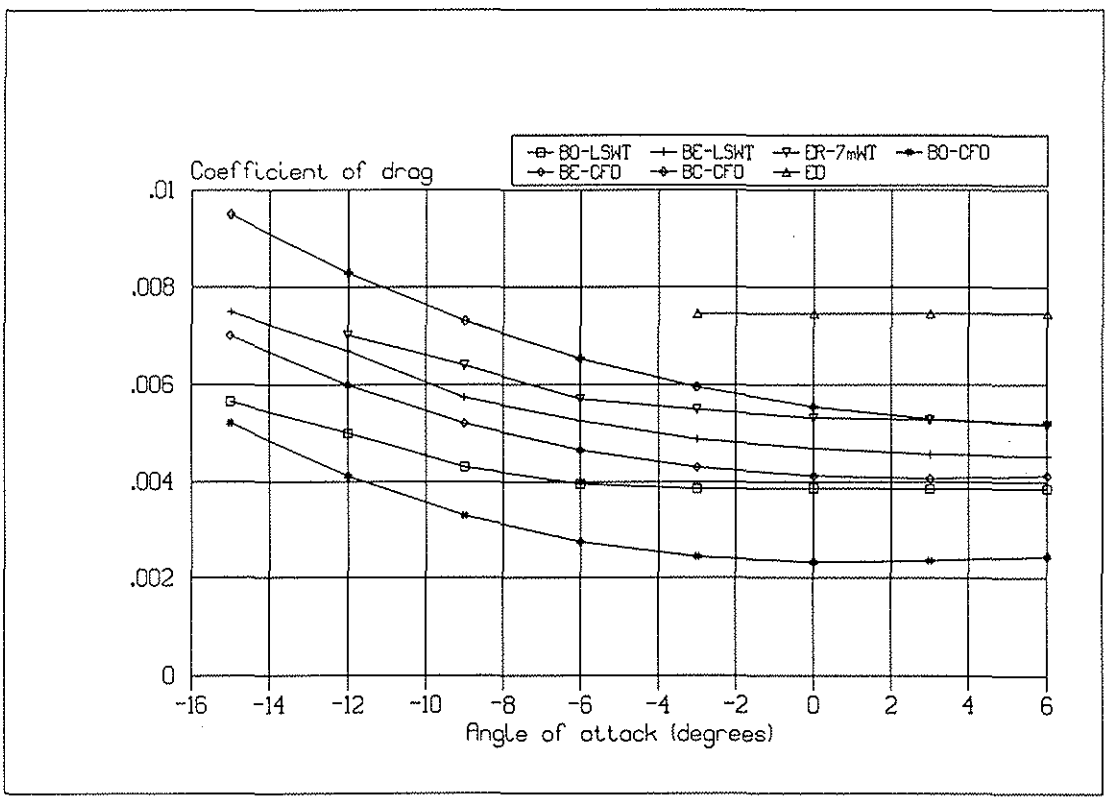

Figure 15: Coefficient of drag variation with angle of attack for the zero yaw conditions.

5 CONCLUSIONS

Three-dimensional models for the simulation of flow around the Alouette III fuselage, with the engine as well as with an engine cowl have been developed. The models have been shown to be able to simulate the dominant physics of the problem. The models have also been validated using experimental data, both scaled and full-scale, and the predicted drag and lift were considered to be within expected experimental errors. More detailed validation would be necessary to develop confidence in this type of model. This model shows great promise for extracting aerodynamic performance of fuselage changes and allows the designer to extract detailed flow information which would be expensive to determine experimentally. The proposed future direction of the fuselage model would be to complete further validation and then extend it to include the dominant interaction effects such as the main rotor, tail rotor, landing gear, engine and empennage.

6 REFERENCES

1) J. Seddon, Basic Helicopter Aerodynamics, AIAA Education Series, Blackwell London 1990.

2) W. Johnson, A Comprehensive analytical model of rotorcraft aerodynamics and dynamics:
3) Part I - Analysis development, NASA TM 81182, Part II - Users manual, NASA TM 81182,
4) Part II - Program manual, NASA TM 81184 June 1980.

5) D. R. Clark, An Analysis of Airframe/Rotor Interference in Forward Flight, 7th European Rotorcraft and Powered Lift Aircraft Forum, 1981

6) G. Polz and J Quentin, Separated Flow Around Helicopter Bodies, 7th European Rotorcraft and Powered Lift Aircraft Forum, 1981

7) P. F. Sheridan and R.P. Smith, Interactional Aerodynamics - A New Challenge to Helicopter Technology, 35th Annual Forum of the AHS, 1979.

8) P. G. Wilby, C. Young and J. Grant, An Investigation of the Influence of Fuselage Flow Field on Rotor Loads, and the Effects of Vehicle Configuration, 4th European Rotorcraft and Powered Lift Aircraft Forum, 1978

9) H. Huber and G. Polz, Studies on blade-to-blade and rotor-fuselage-tail interferences, AGARD-CP-334, London 1982.

10) J. Steger and R. F. Warming, Flux Vector Splitting of the Inviscid Gas Dynamic Equations with the Application to Finite Difference Methods, J. Comp. Phys., Vol. 40, pp. 263-293, 1981.

11) T. H. Pulliam, Efficient Solution Methods for the Navier-Stokes Equations Lecture Notes for the Von Karman Institute for Fluid Dynamics Lecture Series: Numerical Techniques for Viscous Flow Computation in Turbomachinery Bladings, January 20-24, 1986, Brussels, Belgium.

12) J. F. Thompson, F. C. Thames and C. W. Mastin, Automatic Numerical Generation of Body-Fitted Curvilinear Co-ordinate Systems for Field Containing Any Number of Arbitrary Two-Dimensional Bodies, J. Comp. Phys. vol. 15, no. 3, July 1974.

ACKNOWLEDGEMENTS

The author would like to acknowledge the following people for their contribution to the investigation. P J Lake for the three-dimensional grid generation, I M A Gledhill for the three-dimensional boundary conditions, D C Oakes for the computer runs and data extraction, and M A Honman for general computer support.